Broadband directional scattering through a phase difference acquired in composite nanoparticles

Kotte, T. P.S.; Adam, A. J.L.; Zuidwijk, T.; Heerkens, C. T.H.; Xu, M.; Urbach, H. P.

DOI
10.1364/OE.498461

Publication date
2023

Document Version
Final published version

Published in
Optics Express

Research Article Vol. 31, No. 23 / 6 Nov 2023 / Optics Express 38815
Optics EXPRESS

Broadband directional scattering through a phase difference acquired in composite nanoparticles

T. P. S. Kotte,[1,*] A. J. L. Adam,[1] T. Zuidwijk,[1] C. T. H. Heerkens,[1] M. Xu,[2] and H. P. Urbach[1]

[1]TU Delft, Applied Physics, Optics Research Group, Lorentzweg 1, 2628CJ, Netherlands
[2]TNO, Stieltjesweg 1, 2628CK, Netherlands
[*]t.p.s.kotte@tudelft.nl

Abstract: We study the broadband scattering of light by composite nanoparticles through the Born approximation, FEM simulations, and measurements. The particles consist of two materials and show broadband directional scattering. From the analytical approach and the subsequent FEM simulations, it was found that the directional scattering is due to the phase difference between the fields scattered by of each of the two materials of the nanoparticle. To confirm this experimentally, composite nanoparticles were produced using ion-beam etching. Measurements of SiO_2 / Au composite nanoparticles confirmed the directional scattering which was predicted by theory and simulations.

1. Introduction

Directing light is essential for many modern technologies, from producing computer chips using lithography, to detecting obstacles with LIDAR. Advances in nanofabrication techniques have made it possible to redirect light at the nanoscale. Particles of sizes comparable to the wavelength of the light can be produced to exhibit resonances which determine the direction of the scattered light. This gives rise to exciting properties, for example zero-backscattering for silicon nanospheres [1]. The shape and material of these particles can be changed to customize the scattering properties. Examples include nanoantennas [2–4], (almost) non-radiating particles [5], increased absorption in silicon [6], directional emitters [7], and metalenses [8–10].

The scattering of light by a single particle is mainly determined by the multipole resonances within the nanoparticle. These resonances can be tuned by changing the geometry and material of the nanoparticle or the surrounding medium to obtain a desired scattering pattern [2,11–18]. Another method which has been suggested is changing the illumination conditions [19]. The downside of relying on these resonances for low-index particles is that they largely overlap, resulting in generic Mie scattering. High-index particles have a different disadvantage: the resonances are so sharp that the scattering pattern changes rapidly over a limited bandwidth [1,20].

Most studies have focused on particles made up of a single material. Placing particles of different materials close together allows for more degrees of freedom. Using this freedom, broadband forward and backward scattering has been realised [21–23]. Moreover, directional scattering that is not into the forward and backward direction has been demonstrated for dimer and trimer structures [24–27]. However, the directional scattering by these configurations is a result of the interference between their different constituents where the phase difference is determined by their separation distance. This causes the scattering to significantly depend on the wavelength of the light. Therefore, broadband light scattering outside of backward and forward scattering is hard to attain.

#498461 https://doi.org/10.1364/OE.498461
Journal © 2023 Received 22 Jun 2023; revised 23 Aug 2023; accepted 23 Aug 2023; published 1 Nov 2023

Optics EXPRESS

Alternatively, directional scattering over a broad bandwidth can be achieved by composite nanoparticles. In this work we consider nanoparticles which consist of two distinct region made up of a single material as shown in Fig. 1. The phase difference then only originates from the different materials that are used, in contrast to dimer and trimer configurations. Consequently, these nanoparticles can be designed to function over a broad bandwidth. Constructive and destructive interference between the scattering contributions of the constituents can then be utilised to achieve directional scattering. We will show that this can lead to broadband behaviour.

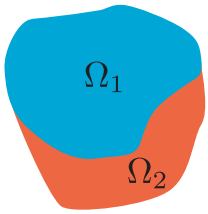

Fig. 1. A composite nanoparticle comprised of two closed volumes Ω_1 and Ω_2, each volume is composed of a different material.

First, a mathematical description is given of the origin of this phase difference. Then the consequences are drawn for core-shell nanoparticles. Because these particles are completely symmetric, the scattering pattern must also be completely symmetric with respect to the polarization of the incident field. In order to break the symmetry, other geometries like core-semishell nanoparticles are considered.

2. Methods

Several methods can be used to determine the scattering by a nanoparticle. For infinite cylinders and spheres, an analytical solution exists in the form of (extended) Mie theory [28,29]. For more complicated geometries, one generally relies on numerical methods because no analytical solution is available. These include the finite element method (FEM), the T-matrix method [30], the discrete dipole approximation [31], resonant state expansion [32], and the Born series [33].

We will start our discussion with a different method, namely the Lippmann-Schwinger integral equation [34]. The reason we start here, is that the scattered field is expressed as an integral over the electric field inside the scatterer. Initially, we will use a few approximations to get some understanding from where the directional scattering originates. Later, we will use FEM to calculate the fields for cases where the approximations do not hold anymore. The Lippmann-Schwinger integral equation (without approximations) is then used to determine the scattered field by the individual parts of the composite particle.

Let us consider a nanoparticle inside of a homogeneous medium. We will denote the space occupied by this particle as Ω. The relative permittivity with respect to vacuum of the particle and the medium is given by $\varepsilon(\boldsymbol{r})$, which is assumed to be isotropic. For convenience, we will use a spherical coordinate system with radial distance r, polar angle θ and azimuthal angle ϕ. The incident electric field is given by $\boldsymbol{E}^{\text{inc}}$. Neglecting polarization effects, the total field as function of the position vector $\boldsymbol{r}$ can then be written as

$$\boldsymbol{E}(\boldsymbol{r}) = k^2 \int_{\Omega} G(\boldsymbol{r}, \boldsymbol{r_0})(\varepsilon(\boldsymbol{r_0}) - \varepsilon_{\text{med}})\boldsymbol{E}(\boldsymbol{r_0}) d^3 r_0 + \boldsymbol{E}^{\text{inc}}(\boldsymbol{r}), \tag{1}$$

where k is the wavenumber in the medium, ε_{med} the permittivity of the medium, $\boldsymbol{E}$ the electric field vector, $\boldsymbol{r_0}$ the position vector over which is integrated, and $G(\boldsymbol{r}, \boldsymbol{r_0})$ the Green's function

Optics EXPRESS

which is given by

$$G(\boldsymbol{r},\boldsymbol{r_0}) = \frac{\exp(ik|\boldsymbol{r}-\boldsymbol{r_0}|)}{4\pi|\boldsymbol{r}-\boldsymbol{r_0}|} \approx \frac{\exp(ik|\boldsymbol{r}-\boldsymbol{r_0}|)}{4\pi r} \tag{2}$$

for large $\boldsymbol{r}$.

We would like to consider a particle made up of two different materials (as shown in Fig. 1). Therefore, we will split up the integral in two different parts: Ω_1 and Ω_2. Only considering the scattering term, we get

$$\begin{aligned}\boldsymbol{E}^{\mathrm{sc}}(\boldsymbol{r}) = k^2 \int_{\Omega_1} G(\boldsymbol{r},\boldsymbol{r_0})(\varepsilon_1 - \varepsilon_{\mathrm{med}})\boldsymbol{E}(\boldsymbol{r_0})d^3r_0 \\ + k^2 \int_{\Omega_2} G(\boldsymbol{r},\boldsymbol{r_0})(\varepsilon_2 - \varepsilon_{\mathrm{med}})\boldsymbol{E}(\boldsymbol{r_0})d^3r_0.\end{aligned} \tag{3}$$

If the internal fields of the particle are known, this equation can be solved, obtaining the scattered field of each part of the particle. Later, we will use FEM to calculate these fields for particles that do not abide to the upcoming approximations.

For now, we will assume that the particle has a very low contrast compared to the medium, such that

$$|\varepsilon_i - \varepsilon_{\mathrm{med}}|kL \ll 1, \text{ where } i = 1, 2, \tag{4}$$

with L the characteristic length of the particle. In this case, we can use the first Born approximation (i.e. $\boldsymbol{E}(\boldsymbol{r_0}) = \boldsymbol{E}^{\mathrm{inc}}(\boldsymbol{r_0})$ inside the integral), avoiding the need to know the exact internal field of the particle, so that

$$\begin{aligned}\boldsymbol{E}^{\mathrm{sc}}(\boldsymbol{r}) = k^2 \int_{\Omega_1} G(\boldsymbol{r},\boldsymbol{r_0})(\varepsilon_1 - \varepsilon_{\mathrm{med}})\boldsymbol{E}^{\mathrm{inc}}(\boldsymbol{r_0})d^3r_0 \\ + k^2 \int_{\Omega_2} G(\boldsymbol{r},\boldsymbol{r_0})(\varepsilon_2 - \varepsilon_{\mathrm{med}})\boldsymbol{E}^{\mathrm{inc}}(\boldsymbol{r_0})d^3r_0.\end{aligned} \tag{5}$$

When a plane wave traveling in the x-direction is incident on the nanoparticle,

$$\boldsymbol{E}^{\mathrm{inc}}(\boldsymbol{r_0}) = \boldsymbol{E_0}\exp(ikr_0\sin\theta_0\cos\phi_0), \tag{6}$$

we get

$$\begin{aligned}\boldsymbol{E}^{\mathrm{sc}}(\boldsymbol{r}) = k^2 \int_{\Omega_1} G(\boldsymbol{r},\boldsymbol{r_0})(\varepsilon_1 - \varepsilon_{\mathrm{med}})\boldsymbol{E_0}\exp(ikr_0\sin\theta_0\cos\phi_0)d^3r_0 \\ + k^2 \int_{\Omega_2} G(\boldsymbol{r},\boldsymbol{r_0})(\varepsilon_2 - \varepsilon_{\mathrm{med}})\boldsymbol{E_0}\exp(ikr_0\sin\theta_0\cos\phi_0)d^3r_0.\end{aligned} \tag{7}$$

The phase term in the Green's function can be simplified for large r by

$$|\boldsymbol{r}-\boldsymbol{r_0}| \approx r\left\{1 - \frac{r_0}{r}\Big[\cos(\phi-\phi_0)\sin\theta\sin\theta_0 + \cos\theta\cos\theta_0\Big] + O\left(\frac{r_0^2}{r^2}\right)\right\}. \tag{8}$$

From here, we will only consider the forward direction: $\phi = 0, \theta = \frac{\pi}{2}$. In this case, we can simplify Eq. (7) as follows:

$$\boldsymbol{E}^{\mathrm{sc}}(r,0,\pi/2) = \boldsymbol{E_0}\frac{k^2\exp(ikr)}{4\pi r}\Big[(\varepsilon_1 - \varepsilon_{\mathrm{med}})\int_{\Omega_1} d^3r_0 + (\varepsilon_2 - \varepsilon_{\mathrm{med}})\int_{\Omega_2} d^3r_0\Big]. \tag{9}$$

The resulting integrals are simply the volumes that the different parts of the nanoparticle occupy. Therefore, the phase difference between the integrals - and therefore the scattered fields of the two parts of the nanoparticle - is only governed by the $(\varepsilon_i - \varepsilon_{\mathrm{med}})$ terms. A phase difference of π can be achieved by either choosing the constituent materials so that the electric permittivity of the medium is in between that of the different constituents in the lossless case. Other phase differences can be achieved by using materials with complex permittivity.

Optics EXPRESS

3. Beyond the Born approximation

To check whether this phase difference is as predicted by the first Born approximation, we will consider particles with increased contrast, for which Eq. (4) does not hold.

As a test case, a core-shell nanoparticle with inner radius of $R = 120$ nm and shell thickness $H = 30$ nm was used. We choose these dimensions so the volumes of the core and shell are approximately equal. For the permittivity of the surrounding medium, we choose $\varepsilon_{\text{med}} = 2$ ($n_{\text{med}} = 1.42$). Taking $\varepsilon_{\text{core}} = 1$ and $\varepsilon_{\text{shell}} = 3$, the contrast ($\varepsilon_i - \varepsilon_{\text{med}}$) is equal and opposite. Because the volumes of the core and shell are approximately equal, the magnitude of the scattered field will be comparable. From Eq. (9), we see that this allows for the scattered field of each part to interfere most effectively.

Next, using the FEM software COMSOL, we simulate an incident plane-wave with a wavelength (in vacuum) of $\lambda_0 = 500$ nm, which is polarized along the z-direction as shown in Fig. 2. From the calculated far field magnitude of the full particle shown in Fig. 3(a), we see this results in side-scattering and decreased forward scattering (for details on the simulation, see supplementary materials).

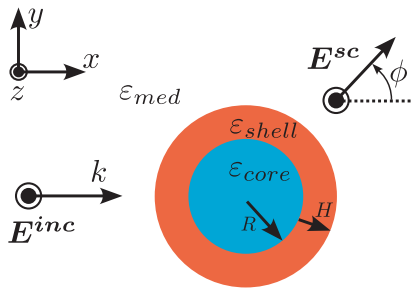

Fig. 2. Plane wave incident on a core-shell nanoparticle with core relative permittivity $\varepsilon_{\text{core}}$ and shell relative permittivity $\varepsilon_{\text{shell}}$. The particle is in a homogeneous space with relative permittivity ε_{med}.

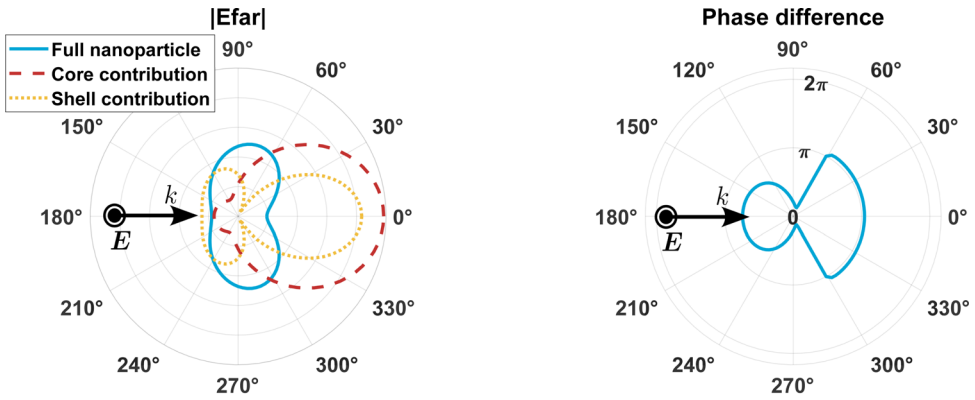

(a) (b)

Fig. 3. Polar plots of (a) the magnitude and (b) phase difference of the light with $\lambda_0 = 500$ nm scattered by a coreshell particle with $\varepsilon_{\text{core}} = 1$, $\varepsilon_{\text{shell}} = 3$, $R = 120$ nm, $H = 30$ nm inside a medium with $\varepsilon_{\text{med}} = 2$.

Since COMSOL does not offer a method to calculate the individual contributions of the core and shell to the total scattering directly, the integrals in Eq. (3) are used to determine this.

Optics EXPRESS

The resulting far field scattering pattern and phase difference of the scattered field between the constituents of the particle is shown in Fig. 3. It can be seen that the scattering pattern of the core and shell resembles Mie scattering by low-index particles: most of the light is scattered in the forward direction and some of the light is scattered backwards. The phase difference explains the scattering pattern for the complete particle: the side-scattering originates from the destructive interference in the forward cone, where the phase difference is almost equal to π. In the sideward directions ($\phi = 100^o$ and $\phi = 260^o$), the phase difference is nearly zero, resulting in constructive interference.

Since the scattering pattern originates directly from the material properties and not from strong multipole resonances, it does not significantly change over the visible spectrum when low dispersive materials are used. The scattering in the forward direction is suppressed over the entire spectrum, resulting in two lobes. On the other hand, the size of the particle compared to the wavelength is important for the scattering cross section. As a result, while the shape of the scattering pattern remains largely the same, the amount of light scattered by the particle decreases with increasing wavelength. To illustrate this, Fig. 4(a) shows the scattering pattern and Fig. 4(b) shows the scattering cross section of the same particle for several wavelengths covering the range of the visible spectrum.

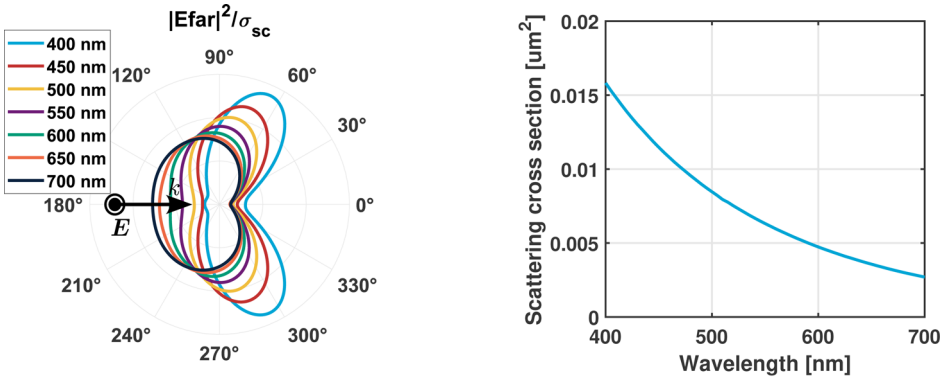

(a) (b)

Fig. 4. Plots of (a) the scattered far field intensity normalized by the scattering cross section and (b) scattering cross section over the visible spectrum of a core-shell nanoparticle in which a π phase difference is introduced between the scattered light of the core and the shell in the forward direction. The same particle is considered as in Fig. 3.

Introducing a material with complex permittivity makes it possible to achieve other phase differences. Now, we maintain the permittivity of the core ($\varepsilon_{\text{core}} = 1$), and change the permittivity of the shell to $\varepsilon_{\text{shell}} = 2 + i$, such that $\varepsilon_{\text{core}} - \varepsilon_{\text{med}} = 1$, and $\varepsilon_{\text{core}} - \varepsilon_{\text{med}} = i$. From Eq. (9), we expect a phase difference of $3\pi/4$ in the forward direction. The results from the simulations, which are shown in Fig. 5, confirm this.

Coincidentally, we see that the scattered field in the backward direction is suppressed over the entire visible spectrum. The same decrease of scattering cross section with wavelength occurs as for the example with materials with only real permittivity for materials with complex permittivity as can be seen in Fig. 6.

It should be noted that it is quite surprising that the discussed theory is still able to give a qualitative understanding of the origin of the directional scattering that is shown here. Clearly, the approximation of Eq. (4) is not valid for these results. While Eq. (7) is not valid, the resulting phase differences, compared to the exact result of Eq. (3), appears to not significantly differ for the range of permittivity and sizes considered in this paper.

Optics EXPRESS

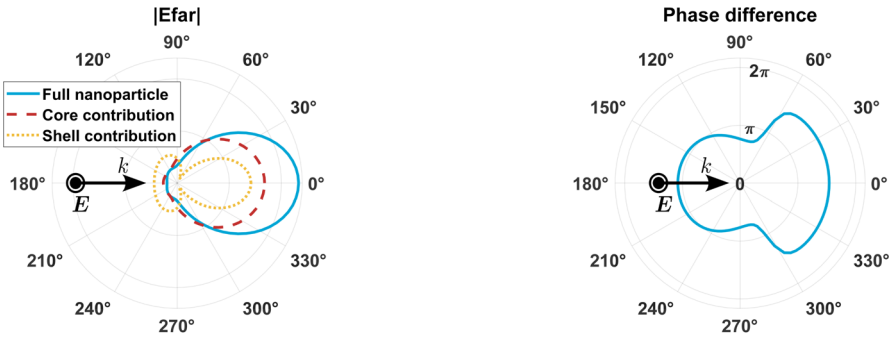

(a) (b)

Fig. 5. Polar plots of (a) the far field magnitude and (b) phase difference of the light with $\lambda_0 = 500$ nm scattered by a coreshell particle with $\varepsilon_{\text{core}} = 1$, $\varepsilon_{\text{shell}} = 2 + i$, $R = 120$ nm, $H = 30$ nm inside a medium with $\varepsilon_{\text{med}} = 2$.

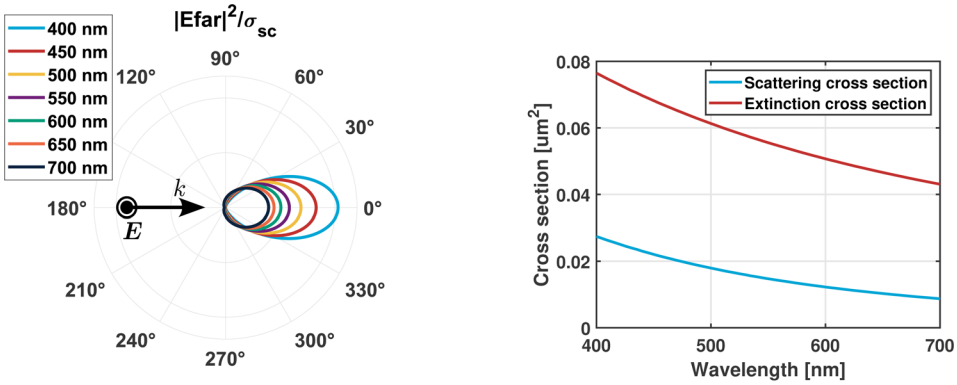

(a) (b)

Fig. 6. Plots of (a) the scattered far field intensity normalized by the scattering cross section and (b) cross sections over the visible spectrum of a core-shell nanoparticle in which a $\pi/2$ phase difference is introduced between the scattered light of the core and the shell in the forward direction. The same particle is considered as in Fig. 5.

4. Anisotropic scattering

In order to facilitate light scattering which is not symmetric around the polarization axis when using isotropic materials, the symmetry of the particle needs to be broken. Therefore, we consider a core-semishell nanoparticle. These type of nanoparticles have already received a considerable amount of attention [35–40], because of their ease of fabrication and to study their geometry dependent resonances.

A plane wave with a wavelength of $\lambda_0 = 500$ nm polarized along the z-direction is incident from the side of the particle, with the semishell placed on the bottom as shown in Fig. 7. We keep the permittivity of the medium the same ($\varepsilon_{\text{med}} = 2$). Then, we sweep over the permittivity of both the core and the semishell and plot the angle at which the magnitude of the scattered light is maximum. For now, we only are interested in the directionality due to the sign difference of $(\varepsilon_i - \varepsilon_{\text{med}})$. Therefore, we will only consider real permittivities.

From the results shown in Fig. 8, we can see that when the permittivity of both the core and the shell is either higher or lower than that of the medium, most light is scattered in the forward

Optics EXPRESS

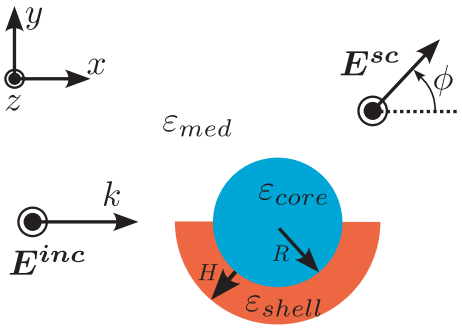

Fig. 7. Schematic of a core-semishell particle with core radius R and semishell thickness H. A planewave is incident from the left of the particle.

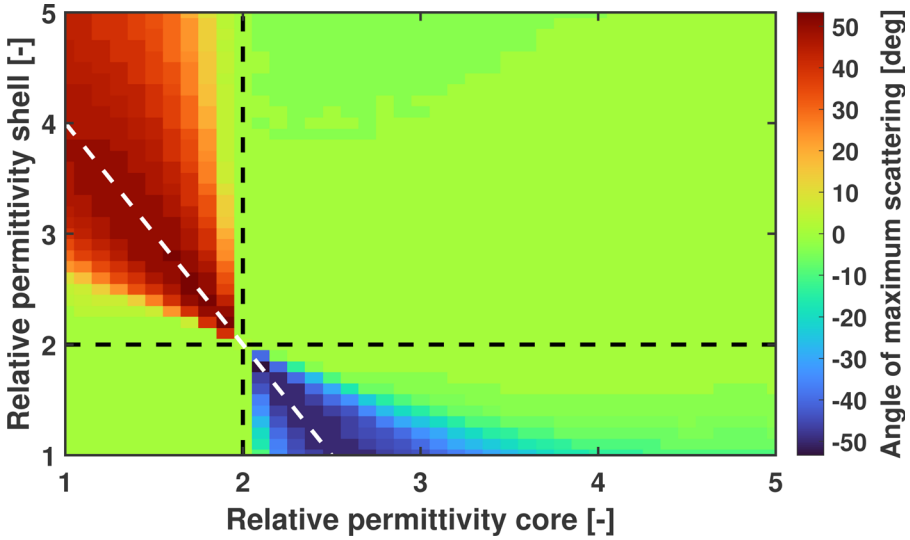

Fig. 8. Angle ϕ of highest magnitude of scattered light with $\lambda_0 = 500$ nm vs core and shell relative permittivity. Core on the horizontal axis and shell on the vertical axis ranging from 1 to 5. The black dashed lines shows the permittivity of the medium ($\varepsilon_{\text{med}} = 2$). Forward scattering is observed unless the permittivity of the medium is in between that of the core and shell. Along the white dashed line, the magnitude of the light scattered by the core and semishell is about equal.

direction. This is consistent with what we have seen before: the non-trivial scattering patterns are found when the permittivity of the core and shell is chosen such that the permittivity of the medium is in between that of the core and shell. Note that the graph only shows the direction of the highest electric far field magnitude, the light is not only scattered in that direction.

For more details, we can look at the actual scattering patterns. In this case we take the permittivity of the core $\varepsilon_{\text{core}} = 1.5$ and the permittivity of the shell $\varepsilon_{\text{shell}} = 3.5$. As seen in Fig. 9, the scattering in the forward direction is almost completely suppressed and the light is scattered to the sides instead. Moreover, for the contributions of the core and shell to interfere properly, the magnitude of the scattered light by each part needs to be comparable. This magnitude is proportional to the volume of a constituent and the contrast. For the geometry considered here (R=120 nm, H=30 nm), the volume of the shell is about half that of the core. Thus, we expect the highest deviation from forward scattering in the case where the contrast of the shell is twice

Optics EXPRESS

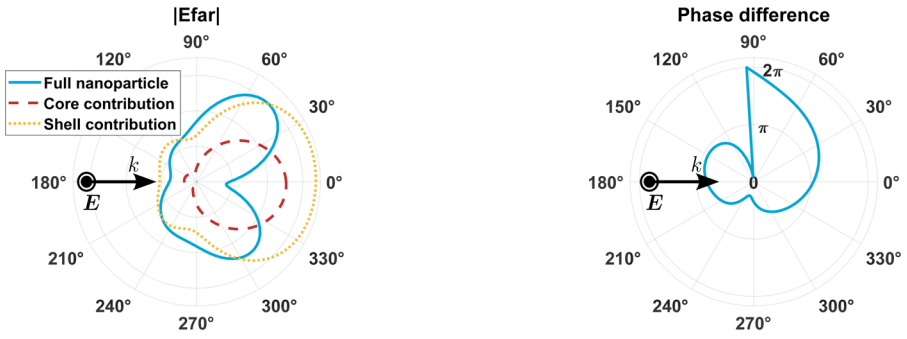

Fig. 9. (a) Far field magnitude and (b) phase difference of light with $\lambda_0 = 500$ nm scattered by a core-semishell particle with $\varepsilon_{\text{core}} = 1.5$, $\varepsilon_{\text{shell}} = 3.5$, $R = 120$ nm, $H = 30$ nm inside a medium with $\varepsilon_{\text{med}} = 2$.

that of the core, which is illustrated by the white dashed line in Fig. 8. Moving away from this condition means that the interference of the scattered field by the core and the shell is not as effective and therefore produces smaller angles.

When using a material with absorption, instead of purely lossless materials, more possibilities arise since it is no longer necessary for the permittivity of the medium to be in between that of the core and the shell to create a phase difference. The complex permittivity of a material is able to introduce interference effects between each part of the nanoparticle. To show this, we again iterate over the permittivity of the core and the shell, but we add an imaginary part to the permittivity of the shell. The relative permittivity of the surrounding medium is kept at $\varepsilon_{\text{med}} = 2$, but the imaginary part of the permittivity of the shell is changed to $\text{Im}\{\varepsilon_{\text{shell}}\} = 1$.

From the results shown in Fig. 10 we can see that, in contrast to the case with lossless components (Fig. 8), directional scattering is achieved for a much larger range of permittivities. The largest angles are again found when the contrast and the volume of the core and the shell are balanced. However, due to absorption the amount of scattered light by the shell is suppressed. As a result, for the cases where the contrast is low (and therefore the imaginary part of the permittivity is relatively high) the scattering angles are smaller.

Furthermore, when looking at the scattering pattern for a particle with $\varepsilon_{\text{core}} = 2.5$ and $\varepsilon_{\text{shell}} = 3 + i$ shown in Fig. 11, we see that the light is scattered into a single direction, as apposed to what we have seen before for the lossless particle in Fig. 9. Of course, since the permittivity of the shell is complex, losses are associated with it because light is absorbed by the particle. This could be a disadvantage in certain applications.

The angle at which the light is scattered, can be controlled through the size of the composite nanoparticle. To show this, we start with the conditions where the scattering angle is greatest. For the lossless particle, this is where the contrast of the core and shell is balanced such that the magnitude of the scattered field of both are about equal. From here, we can change the size of the core and scale the semishell along with it, such that this balance is maintained. The calculated angle at which most light is scattered as a function of the size of the particle is shown in Fig. 12.

From the graph, we can see that we can tune the direction the light is scattered into by changing the size of the nanoparticle. However, there are important changes with respect to the scattering pattern associated with that. For smaller core-semishell particles, the scattering pattern is broadened. For larger particles, the pattern becomes more directional. The same dependence can be seen in Fig. 4. Furthermore, because of the semishell the asymmetry of the scattering with respect to the x-axis is increased.

Optics EXPRESS

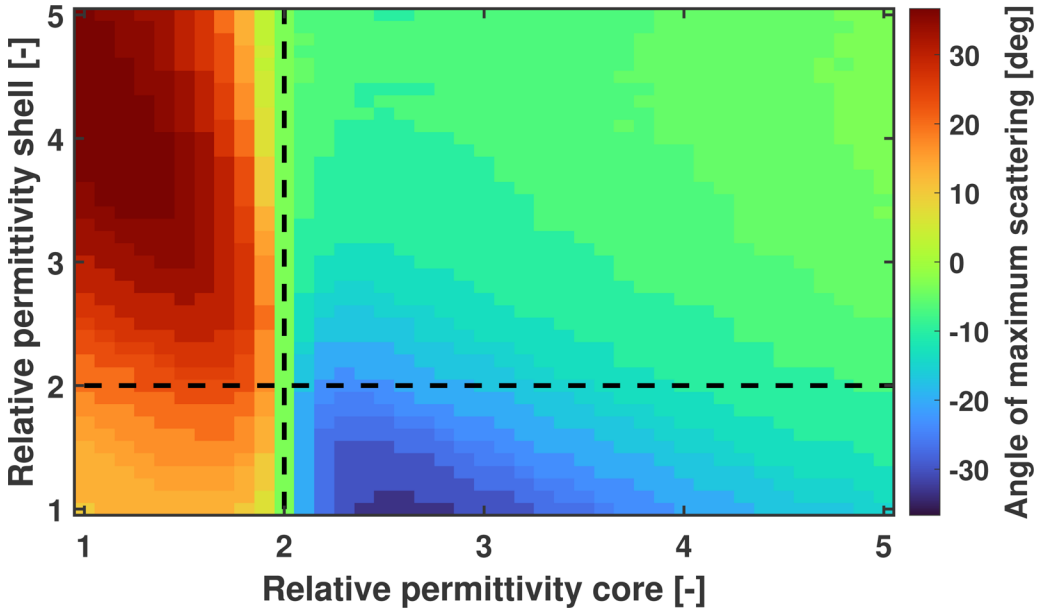

Fig. 10. Angle ϕ of highest magnitude of scattered light with $\lambda_0 = 500$ nm vs core and shell relative permittivity. Core on the horizontal axis and shell on the vertical axis ranging from 1 to 5, the shell has a imaginary part of i.

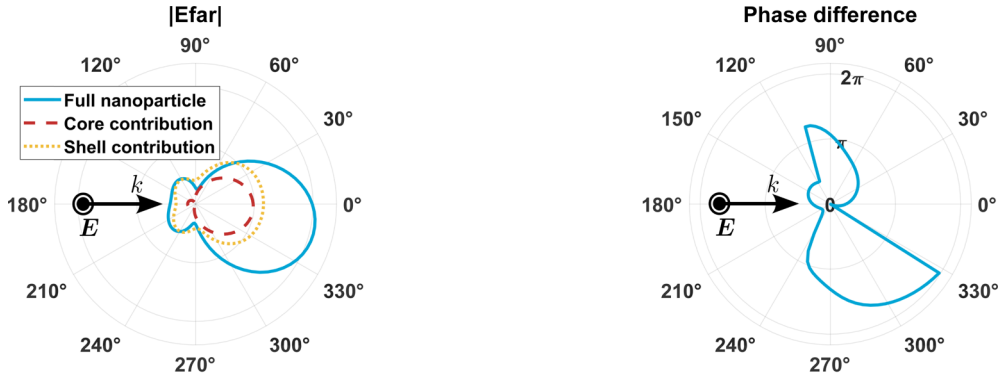

Fig. 11. (a) Far field magnitude and (b) phase difference of light $\lambda_0 = 500$ nm scattered by a core-semishell particle with $\varepsilon_{\text{core}} = 2.5$, $\varepsilon_{\text{shell}} = 3 + i$, $R = 120$ nm, $H = 30$ nm inside a medium with $\varepsilon_{\text{med}} = 2$.

This makes sense in the context of Mie scattering; small particles can only support a limited number of multipole resonances, resulting in a broad scattering pattern. For large particles, more multipole resonances contribute, resulting in more directionality. Specifically for a core radius of 50 nm, the scattering is almost symmetric. Moreover, the large particles barely scatter away from the forward direction.

Here we come to a point where the theory we use to understand the directional scattering breaks down. Up to a core radius of 150 nm, the scattering in the forwards direction is suppressed.

Optics EXPRESS

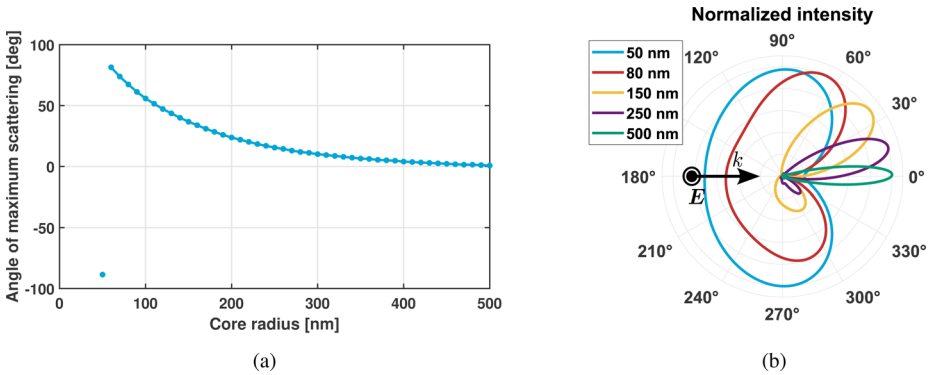

Fig. 12. (a) Angle ϕ of highest magnitude of scattered light with $\lambda_0 = 500$ nm as a function of core radius for a core-semishell particle with $\varepsilon_{\text{core}} = 1$, $\varepsilon_{\text{shell}} = 4$ and $\varepsilon_{\text{med}} = 2$, and (b) related scattering patterns normalized by the maximum intensity.

After this point, the scattering is still directional, but light is scattered in the forward direction. More examples are shown in the supplemental material.

5. Designing a nanoparticle

From the previous sections, we can devise a recipe for the design a nanoparticle with a desired scattering behaviour. To design a nanoparticle which predominantly scatters light in one direction, we use a combination of silica (SiO_2) and gold (Au). Silica nanospheres can be used as one part of the nanoparticle, as they are readily available. If we take spheres with a radius of $R = 150$ nm, using the material permittivities we can calculate the size that the gold part of the nanoparticle should have so the magnitude of the scattered light by the core and the semishell are comparable and can be used to interfere destructively in the forward direction.

An advantage of this method is that the scattering pattern is not very dependent on the geometry of the nanoparticles. As an example, we can consider a nanoparticle which is composed of the same materials, but with a rectangular geometry as shown in Fig. 13. Taking similar size: a nanocube of SiO_2 with sides of length $L = 300$ nm and an attached gold cuboid of the same size except for one side with thickness $T = 24$ nm, Fig. 14 shows that the scattering pattern for this cuboid geometry is very similar to that of a core-semishell particle.

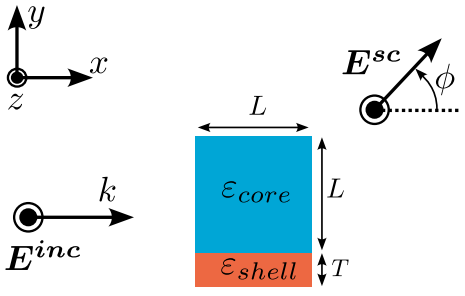

Fig. 13. Schematic of a rectangular particle with side length L and cover thickness T. A planewave is incident from the left of the particle.

Optics EXPRESS

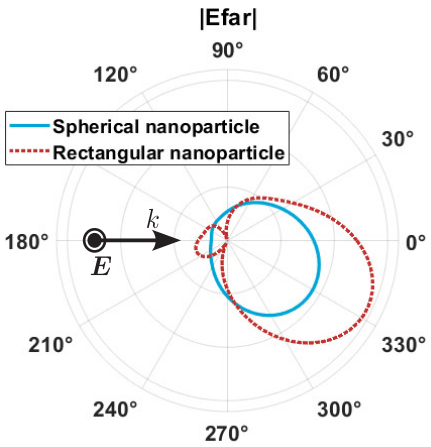

Fig. 14. Far field magnitude of light scattered by a SiO_2 / Au core-semishell particle with $R = 150$ nm, $H = 20$ nm and a rectangular SiO_2 / Au particle with $L = 240$ nm, $T = 40$ nm in air

6. Experimental methods

Using the property that the exact shape is not significant for the scattering pattern, we can design a nanoparticle in a way that the fabrication method is as easy as possible. The shape we have chosen can be seen in Fig. 15(b).

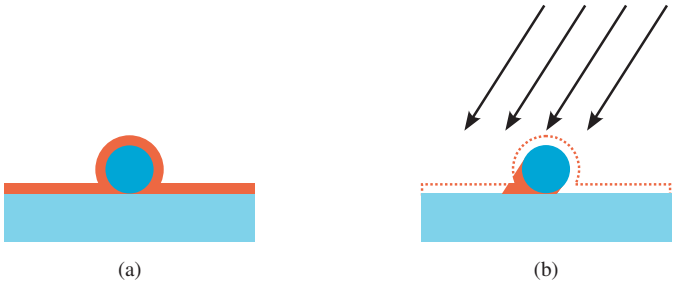

Fig. 15. Fabrication of SiO_2 / Au composite nanoparticles. (a) Result after sputtercoating deposited silica nanospheres with gold and (b) the result after ion beam etching, producing the composite nanoparticle. The arrows indicate the ion beam etching angle.

6.1. Sample fabrication

Glass substrates were cleaned with ethanol and subsequent plasma cleaning. Next, the substrates were covered with a solution of silica nanoparticles suspended in water for 30 min. Then, the glass substrates were thoroughly rinsed with demineralized water and dried using a nitrogen gun. Subsequently, the substrates with the silica nanoparticles were coated with 40 nm of gold through the use of sputter coating. Finally, the nanoparticles were dry etched using an Argon ion beam etcher at an angle of 20 degrees. By etching at an angle, all the gold is removed except for the part that is in the shadow of the spherical silica nanospheres as shown in Fig. 15.

SEM images were taken to check the geometry of the nanoparticles. Figure 16(a) shows an image taken by the SEM from the top, the silica nanosphere is visible with an inner bright ring due to the edge effect. Outside of the nanosphere, the remaining gold part can be seen as a

Optics EXPRESS

brighter circle which is offcenter. Figure 16(b) shows a schematic view of the nanoparticle from the top in the same colors as in Fig. 15.

(a) (b)

Fig. 16. (a) SEM image of a SiO_2 / Au composite nanoparticle. The silica nanosphere can be seen, as well as a the gold part on the left of the sphere, as a result of the etching from the right side and (b) a schematic representation of the particle as seen from above.

6.2. Measurements

The scattering properties of the samples were measured using a HeNe 10 mW laser at 633 nm, of which the light first passed through a beam expander and spatial filter in order to get a clean beam. The laser was focused on the side of the substrate where the nano-particles were deposited, where a spot size of approximately 8 µm was achieved. The laser spot was scanned over the substrate by moving the substrate using a motorized sample stage until a particle was found. The scattered light was then collected by a high-NA (0.85) microscope objective (see Fig. 17 for a schematic of the setup). A second lens after the objective lens was used to create an image. One focal distance after the image plane, another lens was placed to create the Fourier image plane. Here, a mask was placed to block the light that had not scattered. After another focal distance, another lens was placed to focus the light into an image plane. Then, the light is split 90:10 using a beamsplitter cube. For the light that is transmitted (at the 10% side), the object is imaged on a CMOS camera. The light that is reflected (the 90% side) passes through a final lens in order to project the Fourier image on a CMOS camera.

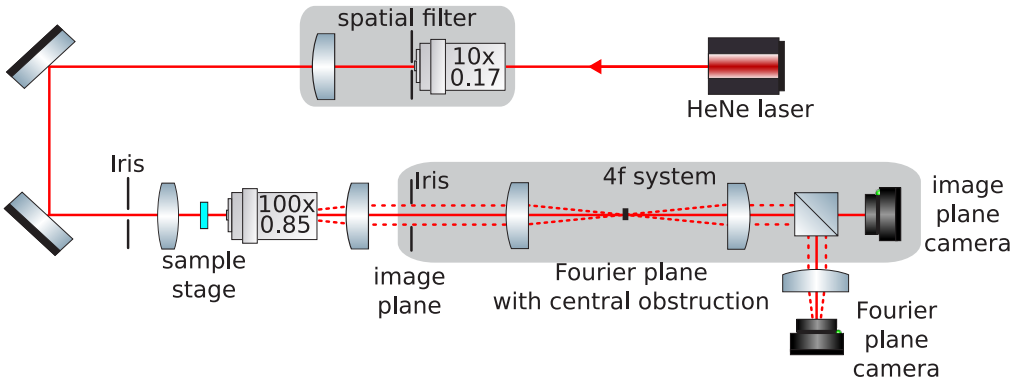

Fig. 17. Schematic of the optical setup, rays coming from the back focal plane are dashed. Note that the back focal plane of the microscope objective is inside of it.

Optics EXPRESS

7. Results and discussion

Measurements on SiO_2 / Au composite nanoparticles are compared to a FEM simulation (see supplemental material for more information). In Fig. 18, the polarization of the incident field is along the *y*-direction, while in Fig. 19 the polarization of the incident field is along the *x*-direction. The orientation of the particle is such that the symmetry axis is perpendicular to the polarization. The cases where these are parallel can be found in the supplemental material.

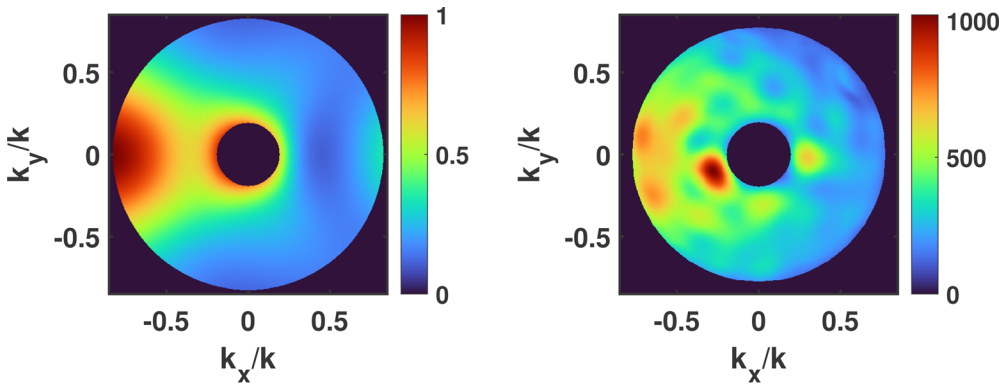

(a) (b)

Fig. 18. (a) Scattered field intensity (Fourier space) as calculated through FEM software, where the polarization of the incident field is along the *y*-direction and the symmetry axis of the particle is along the *x*-direction. (b) As measured using the transmission Fourier microscope setup (arbitrary units).

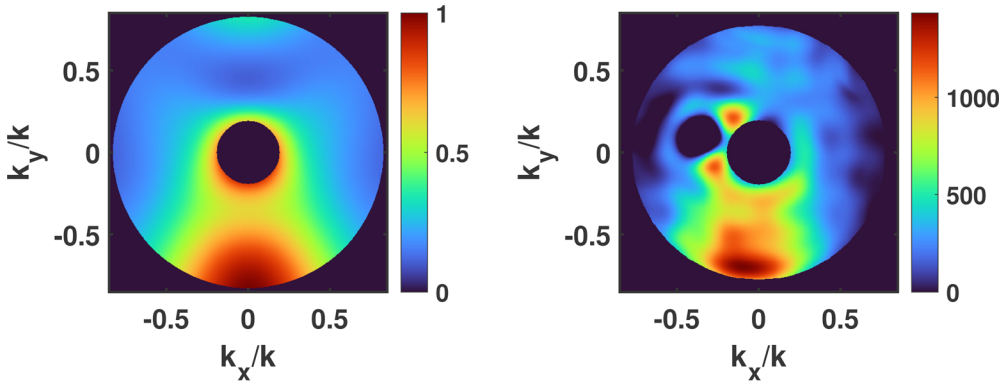

(a) (b)

Fig. 19. (a) Scattered field intensity (Fourier space) as calculated through FEM software, where the polarization of the incident field is along the *x*-direction and the symmetry axis of the particle is along the *y*-direction. (b) As measured using the transmission Fourier microscope setup (arbitrary units).

By rotating the sample and polarization, we can be sure the directional scattering is due to the particle and not due to potential miss-alignments in the optical system. After the rotation, different particles on the same sample were measured due to practical limitations, explaining the

Optics EXPRESS

difference between Fig. 18 and Fig. 19. The figures show the Fourier plane up to the NA of the microscope objective. It is important to note that the increased intensity in the forward direction is due to the presence of the substrate. The central part is obstructed up to the NA of the focal spot on the sample, to ensure the camera does not get saturated by the light that is not scattered by the nanoparticle.

To obtain the measurements as shown in Fig. 18 and Fig. 19, background data was recorded in an area of the sample where no particles were present. Both the data from the background and measurement were Fourier filtered to remove interference effects. After which the background was subtracted from the measurement. This procedure was necessary, because the intensity of the scattered light by the optical components was comparable to that of the nanoparticle.

While the measurements do show directional scattering towards the right, it does not fully agree with the FEM simulations. There are a few reasons why this could be the case. First, the high intensity is located more to the edge of the NA. Because the raw measurement data is Fourier filtered to remove high spatial frequencies, the intensity at the boundary of the NA is reduced. Second, the optical constants used for the materials may deviate from the ones used in the simulations. Furthermore, the procedure for the removal of background signal could have introduced some artifacts. Because the background signal is not constant and also depends on the position of the substrate, there are places where too much or too little of the background signal has been removed. Finally, the FEM simulations assume a plane wave incident normal with respect to the substrate, instead of a focused spot. Therefore, we expect the measurement to be more spread out, as each incident plane wave with an angle shifted from the normal adds a similar shift to the scattering pattern.

8. Conclusion

Using FEM simulations, we have shown that broadband directional scattering can be achieved through the use of phase differences of the light scattered by the different parts of a composite nanoparticle. We have also shown that the angle at which the light is scattered can be controlled by changing the size of the nanoparticle. In the case of lossless materials, the phase difference originates from the sign difference in the contrast of the materials with the surrounding medium. For lossy materials, the phase difference also arises from the imaginary part of the permittivity.

Since the scattering is caused by phase differences, which dependent directly on the materials of the nanoparticle, the geometry of the nanoparticles and the wavelength of the incident light have limited impact on the scattered field distribution. This is advantageous for the fabrication of such nanoparticles.

To confirm the theory, composite SiO_2/Au nanoparticles were fabricated through sputtercoating of deposited nanospheres. These were then ion-beam etched to achieve an asymmetric geometry. Measurements of the scattered field with a Fourier microscope setup shows the directional scattering as predicted by theory and simulations. This shows that directional scattering can be achieved using composite nanoparticles, which are relatively easy to fabricate. This could enable the manufacturing of broadband metamaterials.

Funding. Nederlandse Organisatie voor Wetenschappelijk Onderzoek (NWO) (P15-36).

Disclosures. The authors declare no conflicts of interest.

Data availability. Data underlying the results presented in this paper are not publicly available at this time but may be obtained from the authors upon reasonable request.

Supplemental document. See Supplement 1 for supporting content.

References

1. Y. H. Fu, A. I. Kuznetsov, A. E. Miroshnichenko, Y. F. Yu, and B. Luk'yanchuk, "Directional visible light scattering by silicon nanoparticles," Nat. Commun. **4**(1), 1527 (2013).

Optics EXPRESS

2. N. Li, Y. Lai, S. H. Lam, H. Bai, L. Shao, and J. Wang, "Directional Control of Light with Nanoantennas," Adv. Opt. Mater. **9**(1), 2001081 (2021).
3. A. E. Krasnok, C. R. Simovski, P. A. Belov, and Y. S. Kivshar, "Superdirective dielectric nanoantennas," Nanoscale **6**(13), 7354–7361 (2014).
4. D. Vercruysse, Y. Sonnefraud, N. Verellen, F. B. Fuchs, G. Di Martino, L. Lagae, V. V. Moshchalkov, S. A. Maier, and P. Van Dorpe, "Unidirectional side scattering of light by a single-element nanoantenna," Nano Lett. **13**(8), 3843–3849 (2013).
5. L. Wei, Z. Xi, N. Bhattacharya, and H. P. Urbach, "Excitation of the radiationless anapole mode," Optica **3**(8), 799 (2016).
6. P. D. Terekhov, A. B. Evlyukhin, D. Redka, V. S. Volkov, A. S. Shalin, and A. Karabchevsky, "Magnetic Octupole Response of Dielectric Quadrumers," Laser Photonics Rev. **14**(4), 1900331 (2020).
7. X. Meng, U. Guler, A. V. Kildishev, K. Fujita, K. Tanaka, and V. M. Shalaev, "Unidirectional spaser in symmetry-broken plasmonic core-shell nanocavity," Sci. Rep. **3**(1), 1241 (2013).
8. N. Yu, P. Genevet, M. A. Kats, F. Aieta, J.-P. Tetienne, F. Capasso, and Z. Gaburro, "Light Propagation with Phase Reflection and Refraction," Science **334**(6054), 333–337 (2011).
9. E. Arbabi, A. Arbabi, S. M. Kamali, Y. Horie, and A. Faraon, "Multiwavelength polarization-insensitive lenses based on dielectric metasurfaces with meta-molecules," Optica **3**(6), 628 (2016).
10. A. Arbabi and A. Faraon, "Advances in optical metalenses," Nat. Photonics **17**(1), 16–25 (2023).
11. M. Kerker, D.-S. Wang, and C. L. Giles, "Electromagnetic scattering by magnetic spheres," J. Opt. Soc. Am. **73**(6), 765 (1983).
12. R. Alaee, C. Rockstuhl, and I. Fernandez-Corbaton, "An electromagnetic multipole expansion beyond the long-wavelength approximation," Opt. Commun. **407**, 17–21 (2018).
13. A. B. Evlyukhin and B. N. Chichkov, "Multipole decompositions for directional light scattering," Phys. Rev. B **100**(12), 125415 (2019).
14. E. A. Gurvitz, K. S. Ladutenko, P. A. Dergachev, A. B. Evlyukhin, A. E. Miroshnichenko, and A. S. Shalin, "The High-Order Toroidal Moments and Anapole States in All-Dielectric Photonics," Laser Photonics Rev. **13**(5), 1800266 (2019).
15. H. K. Shamkhi, K. V. Baryshnikova, A. Sayanskiy, P. Kapitanova, P. D. Terekhov, P. Belov, A. Karabchevsky, A. B. Evlyukhin, Y. Kivshar, and A. S. Shalin, "Transverse scattering and generalized kerker effects in all-dielectric mie-resonant metaoptics," Phys. Rev. Lett. **122**(19), 193905 (2019).
16. I. Fernandez-Corbaton, S. Nanz, R. Alaee, and C. Rockstuhl, "Exact dipolar moments of a localized electric current distribution," Opt. Express **23**(26), 33044 (2015).
17. J. Y. Lee, A. E. Miroshnichenko, and R.-K. Lee, "Simultaneously nearly zero forward and nearly zero backward scattering objects," Opt. Express **26**(23), 30393 (2018).
18. P. D. Terekhov, H. K. Shamkhi, E. A. Gurvitz, K. V. Baryshnikova, A. B. Evlyukhin, A. S. Shalin, and A. Karabchevsky, "Broadband forward scattering from dielectric cubic nanoantenna in lossless media," Opt. Express **27**, 10924–10935 (2019).
19. L. Wei, M. F. Picardi, J. J. Kingsley-Smith, A. V. Zayats, and F. J. Rodríguez-Fortuño, "Directional scattering from particles under evanescent wave illumination: the role of reactive power," Opt. Lett. **43**(14), 3393–3396 (2018).
20. D. G. Baranov, D. A. Zuev, S. I. Lepeshov, O. V. Kotov, A. E. Krasnok, A. B. Evlyukhin, and B. N. Chichkov, "All-dielectric nanophotonics: the quest for better materials and fabrication techniques," Optica **4**(7), 814 (2017).
21. H. Wang, P. Liu, Y. Ke, Y. Su, L. Zhang, N. Xu, S. Deng, and H. Chen, "Janus magneto–electric nanosphere dimers exhibiting unidirectional visible light scattering and strong electromagnetic field enhancement," ACS Nano **9**(1), 436–448 (2015).
22. Y. Li, M. Wan, W. Wu, Z. Chen, P. Zhan, and Z. Wang, "Broadband zero-backward and near-zero-forward scattering by metallo-dielectric core-shell nanoparticles," Sci. Rep. **5**(1), 12491 (2015).
23. Y. Chen, S. Chen, T. M. Shih, J. Wang, W. Yang, L. Qian, and Z. Yang, "Broadband unidirectional scattering in visible ranges and controllable hot-spot spatial transfer via a single nanoparticle," Appl. Surf. Sci. **528**, 146489 (2020).
24. P. Albella, T. Shibanuma, and S. A. Maier, "Switchable directional scattering of electromagnetic radiation with subwavelength asymmetric silicon dimers," Sci. Rep. **5**(1), 18322 (2015).
25. G. Lu, Y. Wang, R. Y. Chou, H. Shen, Y. He, Y. Cheng, and Q. Gong, "Directional side scattering of light by a single plasmonic trimer," Laser Photonics Rev. **9**(5), 530–537 (2015).
26. T. Shegai, S. Chen, V. D. Miljković, G. Zengin, P. Johansson, and M. Käll, "A bimetallic nanoantenna for directional colour routing," Nat. Commun. **2**(1), 481 (2011).
27. T. Shibanuma, T. Matsui, T. Roschuk, J. Wojcik, P. Mascher, P. Albella, and S. A. Maier, "Experimental Demonstration of Tunable Directional Scattering of Visible Light from All-Dielectric Asymmetric Dimers," ACS Photonics **4**(3), 489–494 (2017).
28. H. C. Hulst and H. C. van de Hulst, *Light Scattering by Small Particles* (Dover Publications, 1981), Chap. 9.
29. I. L. Rasskazov, P. S. Carney, and A. Moroz, "Stratify: a comprehensive and versatile matlab code for a multilayered sphere," OSA Continuum **3**(8), 2290–2306 (2020).
30. P. C. Waterman, "Symmetry, unitarity, and geometry in electromagnetic scattering," Phys. Rev. D **3**(4), 825–839 (1971).

Optics EXPRESS

31. A. B. Evlyukhin, C. Reinhardt, and B. N. Chichkov, "Multipole light scattering by nonspherical nanoparticles in the discrete dipole approximation," Phys. Rev. B **84**(23), 235429 (2011).
32. S. V. Lobanov, W. Langbein, and E. A. Muljarov, "Resonant-state expansion of three-dimensional open optical systems: Light scattering," Phys. Rev. A **98**(3), 033820 (2018).
33. T. A. Van Der Sijs, O. El Gawhary, and H. P. Urbach, "Electromagnetic scattering beyond the weak regime: Solving the problem of divergent Born perturbation series by Padé approximants," Phys. Rev. Res. **2**(1), 013308 (2020).
34. A. Ishimaru, *Wave Propagation and Scattering in Random Media* (IEEE Press, 1997), Chap. 10.
35. R. Fujimura, R. Zhang, Y. Kitamoto, M. Shimojo, and K. Kajikawa, "Modeling of semi-shell nanostructures formed by metal deposition on dielectric nanospheres and numerical evaluation of plasmonic properties," Jpn. J. Appl. Phys. **53**(3), 035201 (2014).
36. N. A. Mirin and N. J. Halas, "Light-bending nanoparticles," Nano Lett. **9**(3), 1255–1259 (2009).
37. N. A. Mirin, T. A. Ali, P. Nordlander, and N. J. Halas, "Perforated Semishells : Far-Field," ACS Nano **4**(5), 2701–2712 (2010).
38. T. Hinamoto, H. Sugimoto, and M. Fujii, "Metal-Core/Dielectric-Shell/Metal-Cap Composite Nanoparticle for Upconversion Enhancement," J. Phys. Chem. C **122**(30), 17465–17472 (2018).
39. J. Ye, N. Verellen, W. Van Roy, L. Lagae, G. Maes, G. Borghs, and P. Van Dorpe, "Plasmonic modes of metallic semishells in a polymer film," ACS Nano **4**(3), 1457–1464 (2010).
40. M. B. Cortie, J. Giddings, and A. Dowd, "Optical properties and plasmon resonances of titanium nitride nanostructures," Nanotechnology **21**(11), 115201 (2010).